Robust Blind Text Image Deblurring via Maximum Consensus Framework

Zijian Min, Gundu Mohamed Hassan, Geun-Sik Jo*,

Department of Computer Science and Engineering, Inha University, South Korea
minzijian@inha.edu, hazzi@inha.edu, gsjo@inha.ac.kr

Abstract

The blind text image deblurring problem presents a formidable challenge, requiring the recovery of a clean and sharp text image from a blurry version with an unknown blur kernel. Sparsity-based strategies have demonstrated their efficacy by emphasizing the sparse priors of the latent image and kernel. However, these existing strategies have largely neglected the influence of additional noise, imposing limitations on their performance. To overcome this limitation, we propose a novel framework designed to effectively mitigate the impact of extensive noise prevalent in blurred images. Our approach centers around a robust Maximum Consensus Framework, wherein we optimize the quantity of interest from the noisy blurry image based on the maximum consensus criterion. Furthermore, we propose the integration of the Alternating Direction Method of Multipliers (ADMM) and the Half-Quadratic Splitting (HQS) method to effectively address the computationally intractable ℓ_0 norm problem. This innovative strategy enables improvements in the deblurring performance of blurry text images with the additional synthetic noise. Experimental evaluations conducted on various noisy blurry text images demonstrate the superiority of the proposed approach over existing methods.

Introduction

Image deblurring is a low-level computer vision task, where image blur can arise from various sources, such as camera shake (Köhler et al. 2012), object motion (Gong et al. 2017), or defocus (Zhou, Lin, and Nayar 2011).

The problem about recovering a blur kernel and sharp latent image from a blurred image, also known as blind image deblurring, has emerged as a fundamental challenge in the field of image and signal processing. It's been attracting significant attention from the vision and graphics community over the past decade. Numerous research efforts have been devoted to this problem (Nah, Hyun Kim, and Mu Lee 2017; Tao et al. 2018; Chen et al. 2020; Huang, Xia, and Ye 2021; Ji et al. 2022) to improve the quality and fidelity of blurred images. Mathematically, the blur kernel is characterized by the spatial invariance assumption, and as such, the blur process is typically represented by:

$$\boldsymbol{B} = \boldsymbol{L} \otimes \boldsymbol{K} + \boldsymbol{E}, \tag{1}$$

where $\boldsymbol{B}$, $\boldsymbol{L}$, $\boldsymbol{K}$, $\boldsymbol{E}$, $\otimes$ denote the observed blurry image, the corresponding unknown sharp image, unknown kernel, multiple noise, and convolution operator respectively. The problem defined by (1) is considered ill-posed due to the simultaneous unknowns, $\boldsymbol{L}$ and $\boldsymbol{K}$, leading to an infinite number of possible solutions. To address this challenge effectively, additional prior knowledge constraints regarding both kernels and images become imperative.

In contrast to natural-scene imaging, text images exhibit deviations in gradient statistics that do not align with the prior expectations based on heavy-tailed gradient distributions (Pan et al. 2016a). This discrepancy can be attributed to the characteristic two-toned nature (black and white) of text images. Additionally, clear text images manifest more pronounced zero peaks concerning both pixel intensities and gradients when compared to their blurry counterparts. Capitalizing on this inherent characteristic of text images, a framework based on a least squares approximation, integrating diverse sparse priors, has been introduced to effectively address the challenge of text image deblurring (Pan et al. 2016a; Fang et al. 2018; Li et al. 2023).

Nevertheless, within the existing text image deblurring strategies, the influence of additional noise is often overlooked, with the focus primarily centered on the sparse priors of the latent image and kernel. It is essential to acknowledge that such approaches may encounter limitations when dealing with blurred text images that encompass a substantial amount of noise, including both Gaussian and non-Gaussian noise.

To address the challenge of handling the noise in the blurry text image, we put forth a novel maximum consensus framework tailored for robust text image deblurring. This framework facilitates deterministic search within robust fitting problems, with a central objective of segregating inliers from outliers through the maximization of the consensus number of inliers. Nonetheless, the intrinsic complexity of maximum consensus estimation renders exhaustive search indispensable for attaining the global optimum, particularly well-suited when applied to datasets of limited scale. To address this limitation, we further explore the use of the Alternating Direction Method of Multipliers (ADMM) and the Half-Quadratic Splitting (HQS) method. By employing these optimization methods, this deterministically approximate solution is poised to strike a balance between compu-

*Corresponding Author

tational efficiency and solution quality, offering a promising avenue for optimizing the consensus framework.

In summary, this paper makes the following main contributions: (i) Introducing a novel maximum consensus framework for robust text image deblurring, effectively alleviating the impact of noise; (ii) The proposition of a locally convergent solution integrated within the aforementioned framework, which seamlessly amalgamates the ADMM and HQS, thus furnishing a viable way for optimizing our innovative framework. Moreover, the experimental results provide empirical evidence that highlights the efficacy and superiority of the proposed method in comparison to existing approaches for addressing blurry text images with the presence of additional noises.

Related Work

Image deblurring has been studied extensively and numerous algorithms have been proposed. Regarding modern approaches to model construction, the majority of recent techniques can be roughly categorized into two primary groups: optimization-based and learning-based strategy.

In terms of the optimization-based aspect (Krishnan and Fergus 2009; Xu and Jia 2010; Levin et al. 2011; Krishnan, Tay, and Fergus 2011; Vega, Molina, and Katsaggelos 2014; Ravi, Mehta, and Singh 2018), this kind of strategy introduces priors to incorporate uncertain characteristics, ranging from fundamental image geometry in the context of its relation to edge detection and saliency, with the objective, to mitigate the ill-posed nature of blind deconvolution. In learning-based strategy (Chakrabarti 2016; Nah, Hyun Kim, and Mu Lee 2017; Zhang et al. 2018; Kupyn et al. 2019; Zhang et al. 2020), deep learning techniques have been designed for the restoration of single images and video sequences. They rely on synthetic pairs of both sharp and blurry images, leveraging deep learning architectures to estimate the latent sharp image as well as the blur kernel.

Furthermore, a multitude of endeavors (Zhong et al. 2013; Pan et al. 2016b; Dong et al. 2017; Chen et al. 2020) have surfaced to address the challenge of noise within optimization-based image deblurring problems. These methodologies often incorporate tailored heuristics or robust regularization priors, specifically devised to distinguish inliers from prominent outliers prevalent in noisy natural images.

Despite the methods proposed for deblurring generic images, it has been observed that these priors often exhibit reduced effectiveness when applied to scenarios involving rich text. Different from the prior that heavy-tailed gradient statistics commonly found in natural image, text images are better characterized by two-tone distributions. Building upon this distinction, numerous scholars (Cho, Wang, and Lee 2012; Pan et al. 2016a; Qin, Wu, and Li 2018; Fang et al. 2018; Li et al. 2023) have introduced innovative sparsity-based priors tailored to both blur kernels and latent images. However, existing text deblurring methods have not explicitly considered the influence of diverse noise in the blurry text image. This oversight has the potential to introduce unpredictable variables into the optimization procedure, subsequently impacting the achievement of accurate optima.

While existing sparsity-based methods for text image deblurring demonstrate the capability to recover the latent image and unknown kernel simultaneously, their performance is limited by the absence of intrinsic denoising properties. In contrast, our proposed method excels by simultaneously denoising and deblurring noisy text images. Subsequently, we provide a comprehensive elucidation of our framework.

Maximum Consensus Framework

The goal of blind deconvolution is to estimate both $\boldsymbol{L}$ and $\boldsymbol{K}$. The general sparsity-based approach to solve this ill-posed problem is least squares approximation, seeking a pair $(\boldsymbol{L}^*, \boldsymbol{K}^*)$ via

$$(\boldsymbol{L}^*, \boldsymbol{K}^*) = \arg\min_{\boldsymbol{L},\boldsymbol{K}} \|\boldsymbol{B} - \boldsymbol{K} \otimes \boldsymbol{L}\|_F^2 + \gamma_K \Psi_K + \gamma_L \Psi_L, \tag{2}$$

where the symbol $\|\cdot\|_F$ represents the Frobenius norm. Additionally, Ψ_K and Ψ_L denote regularization term, associating with the unknown kernel and latent sharp image respectively, with the corresponding coefficients γ_K and γ_L.

Building upon this approach, we subsequently partition the pixel points into distinct inlier and outlier sets. Subsequently, our analysis focuses on a pixel set denoted as $\mathcal{X} = \{\mathcal{I}, \mathcal{O}\}$, where $\mathcal{I}$ denotes the set of inlier pixels, $\mathcal{O}$ denotes the set of outlier pixels. The consensus maximization algorithm is designed to identify the largest consensus set by solving an optimization problem:

$$\begin{aligned} \underset{\boldsymbol{K},\boldsymbol{L}}{\text{maximize}} \quad & |\mathcal{I}| \\ \text{subject to} \quad & \left|(\boldsymbol{K} \otimes \boldsymbol{L})_{ij} - \boldsymbol{B}_{ij}\right| \le \delta, \\ & \forall\, (\boldsymbol{K} \otimes \boldsymbol{L})_{ij} \in \mathcal{I}, \end{aligned} \tag{3}$$

where the pixel value in the i-th row and j-th column of the latent image after filtering are denoted as $(\boldsymbol{K} \otimes \boldsymbol{L})_{ij}$, while $\boldsymbol{B}_{ij}$ refers to the corresponding pixel value in the observed blurry image.

Furthermore, we transform (3) to the complementary problem, where a slack variable $\boldsymbol{S}$ is introduced as follows:

$$\begin{aligned} \underset{\boldsymbol{K},\boldsymbol{L},\boldsymbol{S}}{\text{maximize}} \quad & HW - \|\boldsymbol{S}\|_{0,0} \\ \text{subject to} \quad & \left|(\boldsymbol{K} \otimes \boldsymbol{L})_{ij} - \boldsymbol{B}_{ij}\right| \le \delta + \boldsymbol{S}_{ij}, \\ & \boldsymbol{S}_{ij} \ge 0, \end{aligned} \tag{4}$$

where H and W represent the height and width of the observed image, respectively, and $\|\boldsymbol{S}\|_{0,0}$ denotes the number of non-zero elements in matrix $\boldsymbol{S}$. Moreover, the inequality constraint part in (4) can be expressed as a pair of linear inequality constraints, as shown below:

$$(\boldsymbol{K} \otimes \boldsymbol{L})_{ij} - \boldsymbol{B}_{ij} \le \delta + \boldsymbol{S}_{ij} \tag{5}$$

and

$$-(\boldsymbol{K} \otimes \boldsymbol{L})_{ij} + \boldsymbol{B}_{ij} \le \delta + \boldsymbol{S}_{ij}. \tag{6}$$

Through denoting $\tilde{\boldsymbol{K}} = \left[\boldsymbol{K}^T, -\boldsymbol{K}^T\right]^T$, $\tilde{\boldsymbol{L}} = \left[\boldsymbol{L}^T, \boldsymbol{L}^T\right]^T$, $\tilde{\boldsymbol{B}} = \left[\boldsymbol{B}^T, -\boldsymbol{B}^T\right]^T$, $\tilde{\boldsymbol{S}} = \left[\boldsymbol{S}^T, \boldsymbol{S}^T\right]^T$, and

$\tilde{\boldsymbol{K}} \odot \tilde{\boldsymbol{L}} = \left[(\boldsymbol{K} \otimes \boldsymbol{L})^T, (-\boldsymbol{K} \otimes \boldsymbol{L})^T \right]^T$, the problem (4) can be generalized as

$$\begin{aligned} \underset{\boldsymbol{K},\boldsymbol{L},\boldsymbol{S}}{\text{minimize}} \quad & \|\boldsymbol{S}\|_{0,0} \\ \text{subject to} \quad & \tilde{\boldsymbol{K}} \odot \tilde{\boldsymbol{L}} - \tilde{\boldsymbol{B}} \leq \tilde{\boldsymbol{S}} + \delta \mathbf{1}_{2H \times W}, \\ & \boldsymbol{S} \geq \mathbf{0}, \end{aligned} \tag{7}$$

where $\mathbf{1}_{2H \times W}$ denotes a matrix with dimensions $2H \times W$ wherein all its entries have a uniform value, equal to 1.

Nevertheless, the existence of simultaneous unknowns in this framework gives rise to an infinite number of potential solutions for both $\boldsymbol{L}$ and $\boldsymbol{K}$. To address this issue, we integrate prior knowledge from framework (2) with consensus maximization. Specifically, we adopt the ℓ_0 regularized image intensity and gradient prior as proposed in (Pan et al. 2016a). By incorporating the additional constraints $\Psi_K(\boldsymbol{K}) = \|\boldsymbol{K}\|_F^2 \leq t$, and $\Psi_L(\boldsymbol{L}) = \sigma \|\boldsymbol{L}\|_{0,0} + \|\nabla \boldsymbol{L}\|_{0,0} \leq t$, with t being a sufficiently small constant real number, the Lagrangian reformulation of this optimization problem is as follows:

$$\begin{aligned} \underset{\boldsymbol{K},\boldsymbol{L},\boldsymbol{S}}{\text{minimize}} \quad & \|\boldsymbol{S}\|_{0,0} + \gamma_K \Psi_K(\boldsymbol{K}) + \gamma_L \Psi_L(\boldsymbol{L}) \\ \text{subject to} \quad & \tilde{\boldsymbol{K}} \odot \tilde{\boldsymbol{L}} - \tilde{\boldsymbol{B}} \leq \tilde{\boldsymbol{S}} + \delta \mathbf{1}_{2H \times W}, \\ & \boldsymbol{S} \geq \mathbf{0}. \end{aligned} \tag{8}$$

Optimization Analysis

By introducing an auxiliary variable $\boldsymbol{V} = \left[\boldsymbol{V}_1^T, \boldsymbol{V}_2^T \right]^T$, the problem (8) can be reconfigured in the form of an equality constraint:

$$\begin{aligned} \underset{\boldsymbol{K},\boldsymbol{L},\boldsymbol{S},\boldsymbol{V}}{\text{minimize}} \quad & \|\boldsymbol{S}\|_{0,0} + \gamma_K \Psi_K(\boldsymbol{K}) + \gamma_L \Psi_L(\boldsymbol{L}) \\ \text{subject to} \quad & \tilde{\boldsymbol{K}} \odot \tilde{\boldsymbol{L}} - \tilde{\boldsymbol{B}} - \tilde{\boldsymbol{S}} - \delta \mathbf{1}_{2H \times W} = \boldsymbol{V}, \\ & \boldsymbol{S} \geq \mathbf{0}, \boldsymbol{V} \leq \mathbf{0}, \end{aligned} \tag{9}$$

where $\boldsymbol{V}_1 = \boldsymbol{K} \otimes \boldsymbol{L} - \boldsymbol{B} - \boldsymbol{S} - \delta \mathbf{1}_{H \times W}$ and $\boldsymbol{V}_2 = -\boldsymbol{K} \otimes \boldsymbol{L} + \boldsymbol{B} - \boldsymbol{S} - \delta \mathbf{1}_{H \times W}$ in the constraint part. The corresponding augmented scaled Lagrangian is given by:

$$\begin{aligned} \mathcal{L}_\rho = & \|\boldsymbol{S}\|_{0,0} + \gamma_K \Psi_K(\boldsymbol{K}) + \gamma_L \Psi_L(\boldsymbol{L}) \\ & + \boldsymbol{Tr}\left(\rho \boldsymbol{U}^T \left[\tilde{\boldsymbol{K}} \odot \tilde{\boldsymbol{L}} - \tilde{\boldsymbol{B}} - \tilde{\boldsymbol{S}} - \delta \mathbf{1}_{2H \times W} - \boldsymbol{V} \right] \right) \\ & + \frac{\rho}{2} \left\| \tilde{\boldsymbol{K}} \odot \tilde{\boldsymbol{L}} - \tilde{\boldsymbol{B}} - \tilde{\boldsymbol{S}} - \delta \mathbf{1}_{2H \times W} - \boldsymbol{V} \right\|_F^2, \end{aligned} \tag{10}$$

where $\rho \boldsymbol{U} = \rho \left[\boldsymbol{U}_1^T, \boldsymbol{U}_2^T \right]^T$, with the same matrix block partition as $\boldsymbol{V}$, is the matrix form of the Lagrange multiplier and the scalar $\rho \geq 0$. Furthermore, it can be simplified as:

$$\begin{aligned} \mathcal{L}_\rho = & \|\boldsymbol{S}\|_{0,0} + \gamma_K \Psi_K(\boldsymbol{K}) + \gamma_L \Psi_L(\boldsymbol{L}) - \frac{\rho}{2} \|\boldsymbol{U}\|_F^2 \\ & + \frac{\rho}{2} \left\| \tilde{\boldsymbol{K}} \odot \tilde{\boldsymbol{L}} - \tilde{\boldsymbol{B}} - \tilde{\boldsymbol{S}} - \delta \mathbf{1}_{2H \times W} - \boldsymbol{V} + \boldsymbol{U} \right\|_F^2. \end{aligned} \tag{11}$$

To achieve the optimal solution, we can minimize $\mathcal{L}_\rho$ with respect to the primal variables $(\boldsymbol{K}, \boldsymbol{L}, \boldsymbol{S}, \boldsymbol{V})$, while simultaneously maximizing it with respect to the dual variable $\boldsymbol{U}$ through the use of the dual ascent method. Instead of pursuing a joint minimization strategy, we adopt a Gauss-Seidel fashion, sequentially minimizing the $\mathcal{L}_\rho$ over primal variables to derive the ADMM solution (Boyd et al. 2011).

In this way, the deconvolution procedure is formulated as an optimization problem by iteratively solving for the latent image $\boldsymbol{L}$ and the blur kernel $\boldsymbol{K}$:

$$\boldsymbol{L}^{(k+1)} = \arg\min_{\boldsymbol{L}} \frac{\rho}{2} \left\| \tilde{\boldsymbol{K}}^{(k)} \odot \tilde{\boldsymbol{L}} - \boldsymbol{Y}^{(k)} \right\|_F^2 + \gamma_L \Psi_L, \tag{12}$$

$$\boldsymbol{K}^{(k+1)} = \arg\min_{\boldsymbol{K}} \frac{\rho}{2} \left\| \tilde{\boldsymbol{K}} \odot \tilde{\boldsymbol{L}}^{(k+1)} - \boldsymbol{Y}^{(k)} \right\|_F^2 + \gamma_K \Psi_K, \tag{13}$$

where

$$\boldsymbol{Y}^{(k)} = \left[\left(\boldsymbol{Y}_1^{(k)} \right)^T, \left(\boldsymbol{Y}_2^{(k)} \right)^T \right]^T, \tag{14}$$

with $\boldsymbol{Y}_1^{(k)} = \boldsymbol{B} + \boldsymbol{S}^{(k)} + \delta \mathbf{1}_{H \times W} + \boldsymbol{V}_1^{(k)} - \boldsymbol{U}_1^{(k)}$ and $\boldsymbol{Y}_2^{(k)} = -\boldsymbol{B} + \boldsymbol{S}^{(k)} + \delta \mathbf{1}_{H \times W} + \boldsymbol{V}_2^{(k)} - \boldsymbol{U}_2^{(k)}$.

Concurrently, the updating procedure of the auxiliary variable $(\boldsymbol{S}, \boldsymbol{V})$ and the dual variable $\boldsymbol{U}$ is as follows:

$$\begin{aligned} \boldsymbol{S}^{(k+1)} &= \arg\min_{\boldsymbol{S} \geq \mathbf{0}} \|\boldsymbol{S}\|_{0,0} + \frac{\rho}{2} \left\| \tilde{\boldsymbol{S}} - \boldsymbol{P}^{(k+1)} \right\|_F^2, \\ \boldsymbol{V}^{(k+1)} &= \arg\min_{\boldsymbol{V} \leq \mathbf{0}} \left\| \boldsymbol{V} - \boldsymbol{Q}^{(k+1)} \right\|_F^2, \\ \boldsymbol{U}^{(k+1)} &= \boldsymbol{U}^{(k)} + \tilde{\boldsymbol{K}}^{(k+1)} \odot \tilde{\boldsymbol{L}}^{(k+1)} - \tilde{\boldsymbol{B}} \\ &\quad - \tilde{\boldsymbol{S}}^{(k+1)} - \boldsymbol{V}^{(k+1)} - \delta \mathbf{1}_{2H \times W}, \end{aligned} \tag{15}$$

where

$$\begin{aligned} \boldsymbol{P}^{(k+1)} = & \tilde{\boldsymbol{K}}^{(k+1)} \odot \tilde{\boldsymbol{L}}^{(k+1)} - \tilde{\boldsymbol{B}} \\ & - \delta \mathbf{1}_{2H \times W} - \boldsymbol{V}^{(k)} + \boldsymbol{U}^{(k)} \end{aligned} \tag{16}$$

and

$$\begin{aligned} \boldsymbol{Q}^{(k+1)} = & \tilde{\boldsymbol{K}}^{(k+1)} \odot \tilde{\boldsymbol{L}}^{(k+1)} - \tilde{\boldsymbol{B}} \\ & - \delta \mathbf{1}_{2H \times W} - \tilde{\boldsymbol{S}}^{(k+1)} + \boldsymbol{U}^{(k)} \end{aligned} \tag{17}$$

with matrix block partitions denoted as $\boldsymbol{P} = \left[\boldsymbol{P}_1^T, \boldsymbol{P}_2^T \right]^T$ and $\boldsymbol{Q} = \left[\boldsymbol{Q}_1^T, \boldsymbol{Q}_2^T \right]^T$. These partitions are defined in a manner identical to that of $\boldsymbol{Y}$. In-depth explanations and elaborations of these sub-problems are provided in the subsequent subsections.

Estimating Latent Image $\boldsymbol{L}$

The presence of the ℓ_0 regularization term in (12) renders the minimization of (12) computationally intractable. Inspired by (Pan et al. 2016a), the optimization problem (12) can be solved by the HQS minimization approach (Xu et al. 2011). Specifically, by introducing auxiliary variables $\boldsymbol{J}$ and $\boldsymbol{G} = \left[\boldsymbol{G}_h^T, \boldsymbol{G}_v^T \right]^T$ corresponding to $\boldsymbol{L}$ and $\nabla \boldsymbol{L}$, the problem (12) can reformulated as follows:

$$\begin{aligned} \underset{\boldsymbol{L},\boldsymbol{J},\boldsymbol{G}}{\text{minimize}} \quad & \frac{\rho}{2} \left\| \tilde{\boldsymbol{K}}^{(k)} \odot \tilde{\boldsymbol{L}} - \boldsymbol{Y}^{(k)} \right\|_F^2 + \beta \|\boldsymbol{L} - \boldsymbol{J}\|_F^2 \\ & + \mu \|\nabla \boldsymbol{L} - \boldsymbol{G}\|_F^2 + \gamma_L \left(\sigma \|\boldsymbol{J}\|_{0,0} + \|\boldsymbol{G}\|_{0,0} \right), \end{aligned} \tag{18}$$

where β and μ are hyperparameter. The problem (18) can be efficiently solved through alternatively minimizing the variables $\boldsymbol{L}$, $\boldsymbol{J}$ and $\boldsymbol{G}$ independently while fixing the other variables. Specifically, the optimal value of $\boldsymbol{L}$ is obtained by solving when fixing variables $\boldsymbol{J}$ and $\boldsymbol{G}$:

$$\begin{aligned}\underset{\boldsymbol{L}}{\text{minimize}}\ \frac{\rho}{2}\left\|\tilde{\boldsymbol{K}}^{(k)}\odot\tilde{\boldsymbol{L}}-\boldsymbol{Y}^{(k)}\right\|_F^2+\beta\|\boldsymbol{L}-\boldsymbol{J}\|_F^2\\+\mu\|\nabla\boldsymbol{L}-\boldsymbol{G}\|_F^2,\end{aligned}\tag{19}$$

Moreover, the Convolution Theorem states that convolution in the spatial domain becomes an element-wise multiplication in the Fourier domain. Using the symbol $*_\cdot$ to denote element-wise multiplication and $\mathcal{F}$ to indicate the Fast Fourier Transform (FFT), the closed-form solution of (19) can be expressed as:

$$\boldsymbol{L}^{(k+1)}=\mathcal{F}^{-1}\left(\frac{\rho\boldsymbol{F}_Y+\beta\mathcal{F}\left(\boldsymbol{J}\right)+\mu\boldsymbol{F}_G}{\rho\boldsymbol{F}_K+\beta\mathbf{1}+\mu\boldsymbol{F}_\nabla}\right),\tag{20}$$

where $\boldsymbol{F}_K$, $\boldsymbol{F}_Y$, $\boldsymbol{F}_G$, $\boldsymbol{F}_\nabla$ are defined as $\overline{\mathcal{F}\left(\boldsymbol{K}^{(k)}\right)}*_\cdot\mathcal{F}\left(\boldsymbol{K}^{(k)}\right)$, $\overline{\mathcal{F}\left(\boldsymbol{K}^{(k)}\right)}*_\cdot\left(\mathcal{F}\left(\boldsymbol{Y}_1^{(k)}\right)-\mathcal{F}\left(\boldsymbol{Y}_2^{(k)}\right)\right)/2$, $\overline{\mathcal{F}\left(\nabla_h\right)}*_\cdot\mathcal{F}\left(\boldsymbol{G}_h\right)+\overline{\mathcal{F}\left(\nabla_v\right)}*_\cdot\mathcal{F}\left(\boldsymbol{G}_v\right)$, $\overline{\mathcal{F}(\nabla_h)}*_\cdot\mathcal{F}(\nabla_h)+\overline{\mathcal{F}(\nabla_v)}*_\cdot\mathcal{F}(\nabla_v)$, respectively. Here, ∇_h and ∇_v represent the horizontal and vertical differential operators, correspondingly. Moreover, $\mathcal{F}^{-1}$ and $\overline{\mathcal{F}}$ signify the inverse FFT operator and the complex conjugate operator of the FFT, respectively.

After attaining the optimal value of $\boldsymbol{L}$ in the current iteration, the computation of $\boldsymbol{J}$ and $\boldsymbol{G}$ can be accomplished individually as follows:

$$\begin{aligned}&\underset{\boldsymbol{J}}{\text{minimize}}\ \beta\|\boldsymbol{J}-\boldsymbol{L}^{(k+1)}\|_F^2+\sigma\gamma_L\|\boldsymbol{J}\|_{0,0},\\&\underset{\boldsymbol{G}}{\text{minimize}}\ \mu\|\boldsymbol{G}-\nabla\boldsymbol{L}^{(k+1)}\|_F^2+\gamma_L\|\boldsymbol{G}\|_{0,0},\end{aligned}\tag{21}$$

which corresponds to the identically weighted least squares approximation with an ℓ_0 regularization term, and it can be optimized through the element-wise minimization procedure as follows, with the notation $\boldsymbol{L}^*=\boldsymbol{L}^{(k+1)}$:

$$\boldsymbol{J}_{ij}^*=\begin{cases}\boldsymbol{L}_{ij}^*, & |\boldsymbol{L}_{ij}^*|^2\geqslant\frac{\sigma\gamma_L}{\beta}\\0, & \text{otherwise}\end{cases}\tag{22}$$

and

$$\boldsymbol{G}_{ij}^*=\begin{cases}\nabla\boldsymbol{L}_{ij}^*, & |\nabla\boldsymbol{L}_{ij}^*|^2\geqslant\frac{\gamma_L}{\mu}\\0, & \text{otherwise}\end{cases}\tag{23}$$

Estimating Blur Kernel $\boldsymbol{K}$

With optimal value $\boldsymbol{L}^{(k+1)}$ in the current iteration, we estimate the blur kernel in the gradient space instead of using the form of update (13), influenced by the methodology introduced in (Pan et al. 2016a):

$$\boldsymbol{K}^{(k+1)}=\arg\min_{\boldsymbol{K}}\frac{\rho}{2}\left\|\tilde{\boldsymbol{K}}\odot\tilde{\boldsymbol{L}}_\nabla^{(k+1)}-\boldsymbol{Y}_\nabla^{(k)}\right\|_F^2+\gamma_K\Psi_K,\tag{24}$$

where $\tilde{\boldsymbol{L}}_\nabla^{(k+1)}=\nabla\tilde{\boldsymbol{L}}^{(k+1)}$ and $\boldsymbol{Y}_\nabla^{(k)}=\nabla\tilde{\boldsymbol{B}}+\tilde{\boldsymbol{S}}^{(k)}+\delta\mathbf{1}_{2H\times W}+\boldsymbol{V}^{(k)}-\boldsymbol{U}^{(k)}$. Furthermore, the kernel estimation procedure is executed in a coarse-to-fine strategy by employing an image pyramid. These adjustments yield more precise updates compared to the direct utilization of intensity values, as demonstrated in the algorithm analysis section. Subsequently, problem (24) can also be resolved in a closed-form solution in the Fourier domain. Following the acquisition of the optimal $\boldsymbol{K}^{(k+1)}$, it becomes essential to set negative elements to 0, while simultaneously normalizing the summation of all elements within $\boldsymbol{K}^{(k+1)}$ to 1.

Estimating Auxiliary Variable $(\boldsymbol{S},\boldsymbol{V})$

The optimal update of $\boldsymbol{S}$ becomes computationally intractable due to the presence of $\|\boldsymbol{S}\|_{0,0}$, similar to the complexity observed when updating $\boldsymbol{L}$. To resolve this, we adopt the HQS minimization approach to find the solution for $\boldsymbol{S}$. Specifically, we introduce the second order auxiliary variable $\boldsymbol{H}$ to facilitate the update of $\boldsymbol{S}$, which can be reformulated as follows:

$$\begin{aligned}\boldsymbol{S}^{(k+1)}=\arg\min_{\boldsymbol{S}\geq\mathbf{0},\boldsymbol{H}}\frac{\rho}{2}\left\|\tilde{\boldsymbol{S}}-\boldsymbol{P}^{(k+1)}\right\|_F^2+\|\boldsymbol{H}\|_{0,0}\\+\lambda\|\boldsymbol{S}-\boldsymbol{H}\|_F^2,\end{aligned}\tag{25}$$

whose optimization procedure is partitioned into two regularized least squares approximations, individually, which are alternatively optimized. For optimizing $\boldsymbol{S}$, the optimization problem (25) can be rewritten as follows:

$$\underset{\boldsymbol{S}\geq\mathbf{0}}{\text{minimize}}\ \frac{\rho}{2}\left\|\tilde{\boldsymbol{S}}-\boldsymbol{P}^{(k+1)}\right\|_F^2+\lambda\|\boldsymbol{S}-\boldsymbol{H}\|_F^2,\tag{26}$$

The closed form of $\boldsymbol{S}$ is:

$$\boldsymbol{S}^{(k+1)}=\Pi_{\boldsymbol{S}\geq\mathbf{0}}\left[\frac{\rho\left(\boldsymbol{P}_1^{(k+1)}+\boldsymbol{P}_2^{(k+1)}\right)+2\lambda\boldsymbol{H}}{2\left(\rho+\lambda\right)}\right],\tag{27}$$

where projective function is defined as $\Pi_{\mathcal{C}}(\mathbf{Y})=\arg\min_{\mathbf{X}\in\mathcal{C}}\|\mathbf{X}-\mathbf{Y}\|_F^2$

After obtaining optimal $\boldsymbol{S}^*=\boldsymbol{S}^{(k+1)}$ in the current step, the second order auxiliary variable $\boldsymbol{H}$ is updated via optimizing the following problem:

$$\underset{\boldsymbol{H}}{\text{minimize}}\ \|\boldsymbol{H}\|_{0,0}+\lambda\|\boldsymbol{S}^*-\boldsymbol{H}\|_F^2,\tag{28}$$

which can be optimized on a pixel-wise basis as follows:

$$\boldsymbol{H}_{ij}^*=\begin{cases}\boldsymbol{S}_{ij}^*, & |\boldsymbol{S}_{ij}^*|^2\geqslant\frac{1}{\lambda}\\0, & \text{otherwise}\end{cases}\tag{29}$$

As for updating $\boldsymbol{V}$, it can be efficiently optimized by element-wise projection onto $\mathcal{C}=\{\boldsymbol{V}|\boldsymbol{V}\leq\mathbf{0}\}$:

$$\boldsymbol{V}_{ij}^{(k+1)}=\begin{cases}\boldsymbol{Q}_{ij}^{(k+1)}, & \boldsymbol{Q}_{ij}^{(k+1)}\leqslant 0\\0, & \text{otherwise}\end{cases}\tag{30}$$

Algorithm 1 outlines the procedure for recovering the latent image and unknown kernel within the maximum consensus framework. For the purpose of removing artifacts

Algorithm 1: Robust Text Image Deblurring via Maximum Consensus Framework

Input:
$\boldsymbol{B}$: Blurred image;
$maxIter$: Maximum iteration;
$maxLevel$: Maximum pyramid level;
Output: Intermediate laten image $\boldsymbol{L}^*$ and blur kernel $\boldsymbol{K}^*$.
Process:

```
Build the pyramid images of input blurred image B_i (1 ≤ i ≤ maxLevel) from coarse to fine;
Initialize L_1 = B_1 and K_1;
for i = 1 to maxLevel do
    for k = 1 to maxIter do
        Update L_i^(k) by using (12);
        Update K_i^(k) by solving (24);
        Normalize K_i^(k);
        Update S^(k), V^(k), U^(k) at the current pyramid level by using (15);
    end for
    Upsample B_i and K_i to B_{i+1} and K_{i+1}, respectively;
    Normalize K_{i+1};
end for
L* = L_{maxLevel} and K* = K_{maxLevel};
Return L* and K*.
```

arising due to complex backgrounds or intricate texture details, we integrate the residual deconvolution technique introduced by (Pan et al. 2016a) into each level of the image pyramid. Specifically, we calculate two intermediary latent images denoted as $\boldsymbol{L}_p$ and $\boldsymbol{L}_q$. The former is estimated employing a Laplacian prior strategy (Krishnan and Fergus 2009), while the latter is derived by employing the $\Psi_L(\boldsymbol{L})$ term without the incorporation of intensity regularization. Subsequent to this, we apply a bilateral filter to the difference image between $\boldsymbol{L}_p$ and $\boldsymbol{L}_q$. The eventual result is the refinement of the latent image $\boldsymbol{L}$, achieved through the subtraction of the filtered difference image from $\boldsymbol{L}_p$, effectively reducing any residual ringing artifacts.

Experimental Result

This section provides a thorough performance analysis of our proposed algorithm in contrast to state-of-the-art techniques for text image deblurring, conducted on synthetic image datasets. These methodologies encompass representative strategies, which encompass two sparsity-based approaches and two noise handling methodologies. The brief introduction of the algorithms under comparison is as follows:

- (Zhong et al. 2013): It's a noise handling method for noisy natural blurry images that employs directional filters to mitigate noise while preserving the blur details in their orthogonal direction;
- (Pan et al. 2016a): It's a sparsity-based approach tailored for text blurry images that leverages a potent ℓ_0-regularized prior grounded in both intensity and gradient attributes to address text image deblurring;
- (Chen et al. 2020): It's a noise handling method for noisy natural blurry images that operates by imposing a continuous weighting mask on elements. This mask serves to classify their nature, distinguishing outliers, and subsequently discarding them;
- (Li et al. 2023): It's a sparsity-based approach for text blurry images grounded in the principles of multi-scale fusion and sparse priors, designed to tackle the intricacies of text image deblurring.

During the experimental phase, we set the parameters as follows: $\gamma_L = 4e^{-3}$, $\gamma_K = 2$, and $\sigma = 0.8$.

Quantitative Evaluation on Synthetic Text Images

We employed a dataset comprising 15 authentic text-related images as well as 8 pre-established kernels sourced from (Levin et al. 2009). Employing these kernels, we synthetically generated a collection of blurred images by convolving primary text images, resulting in the creation of 120 distinct blurry image instances. Subsequently, we introduced white Gaussian noise with a standard deviation of 0.1 to each pixel within the images. For the generation of outliers, characterized by heightened noise levels relative to inliers, we intentionally perturbed a randomly selected subset of pixels using Gaussian noise with a standard deviation of 1.2.

Figure 1 presents the average Peak Signal-to-Noise Ratio (PSNR) value for latent image evaluation and kernel similarity for unknown kernel evaluation. The average PSNR value in Figure 1(a) were computed based on 8 kernels for each image, while the average kernel similarity was derived from 15 images for each kernel in Figure 1(b), both with the outlier ratio set at 55%. Given the disruptive influence of outliers, conventional deblurring methods struggle to accurately estimate the blur kernel. Therefore, our comparison primarily focuses on noise handling methodologies in relation to kernel similarity. Additionally, the average PSNR and kernel similarity value in Figure 1(c) and (d) were computed across 120 combinations, varying the proportion of outliers from 0% to 50%.

The quantitative results demonstrate the conspicuously superior performance of our proposed algorithm compared to two sparsity-based methodologies and a noise handling method presented in (Zhong et al. 2013), both in terms of latent image and kernel estimation. In comparison to the noise handling method introduced in (Chen et al. 2020), our proposed method exhibits heightened effectiveness, particularly when the outlier ratio remains under 10%.

Visual Evaluation on Text Blurry Images

Figure 2 presents two representative text blurry instances provided by (Cho, Wang, and Lee 2012), each subject to distinct conditions of noise addition. Specifically, both examples feature a randomly selected subset of pixels exposed to white Gaussian noise with a standard deviation of 1.2. However, the first example is characterized by an outlier proportion of 50%, while the second example exhibits a significantly lower outlier proportion of 10%. The presence

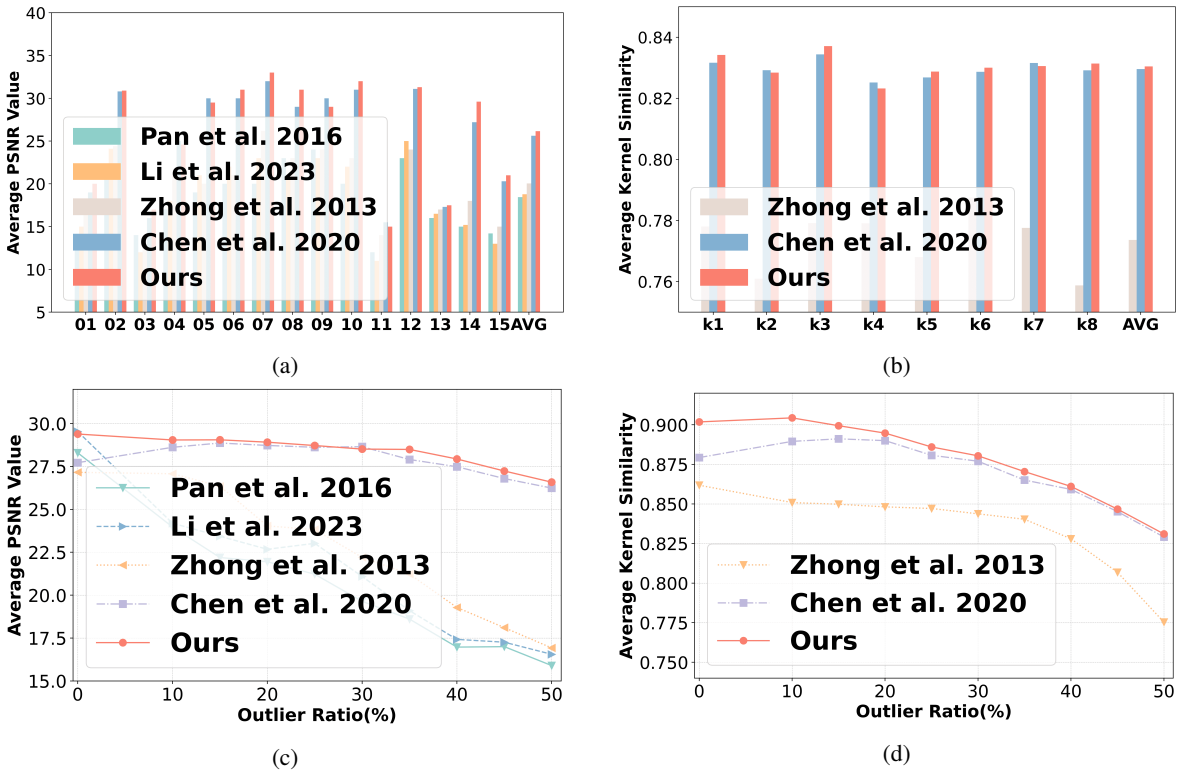

Figure 1: Quantitative analysis of the proposed text image dataset under the influence of additive noise is presented. In (a) and (b), the average PSNR value and kernel similarity are displayed, with an outlier ratio set at 55%. Additionally, (c) and (d) showcase the average PSNR value and kernel similarity across varying outlier ratios, spanning from 0% to 50%.

of outliers significantly impedes the conventional deblurring methods' ability to accurately estimate the blur kernel, reaffirming the conclusions from the quantitative assessment conducted on synthetic text images.

From a perceptual standpoint, our proposed method demonstrates outcomes that are analogous to those presented in (Chen et al. 2020) in the first text example. It is noteworthy that both of these two methods exhibit enhanced performance in comparison to alternative approaches. However, our proposed method engenders visually discernible disparities in comparison to the outcomes obtained from (Chen et al. 2020), as exemplified in the second example, which pertains to scenarios featuring a lower proportion of outliers. We analysis that the observed disparities in outcomes can be attributed to the design focus of (Chen et al. 2020), which is better suited for scenarios characterized by a relatively high proportion of outliers and natural images. In the context of text images, our proposed method emerges as more robust than the approach presented in (Chen et al. 2020).

In the realm of both quantitative and visual evaluation, it becomes apparent that conventional text image deblurring algorithms exhibit a heightened sensitivity to image noise. This susceptibility arises from the underlying framework's lack of emphasis on noise handling considerations. Conversely, noise handling approaches dedicate their algorithmic designs to the domain of natural images and outliers removal. This design choice results in a degree of instability in their performance when applied to the realm of blurry text images characterized by a low proportion of outliers.

Analysis of the Proposed Algorithm

Our proposed estimation algorithm combines the Alternating Direction Method of Multipliers strategy with the Half-Quadratic Splitting minimization approach, primarily employing an alternately optimized procedure.

The convergence rate of our proposed methodology is assessed through the examination of 120 blurred noisy text images. The trajectory about the average energy of the objective function in (2) and the average PNSR value over iterations are depicted in Figure 3(a) and (b), respectively, manifesting a consistent decline and rise until convergence. Both Figure 3(a) and (b) provide empirical evidence of the convergence behavior exhibited by the proposed algorithm.

During the process of latent image and kernel estimation, the data fidelity term in (12) and (13) can be formulated based on either image intensity or gradient level. We systematically assess the efficacy of various combinations involving intensity and gradient applied in (12) and (13). The comparative evaluation is visually represented through Figure 3(c) and (d) with respect to the energy value in (2) and kernel similarity. It is evident from the figures that all combinations exhibit convergence, yet the configuration employ-

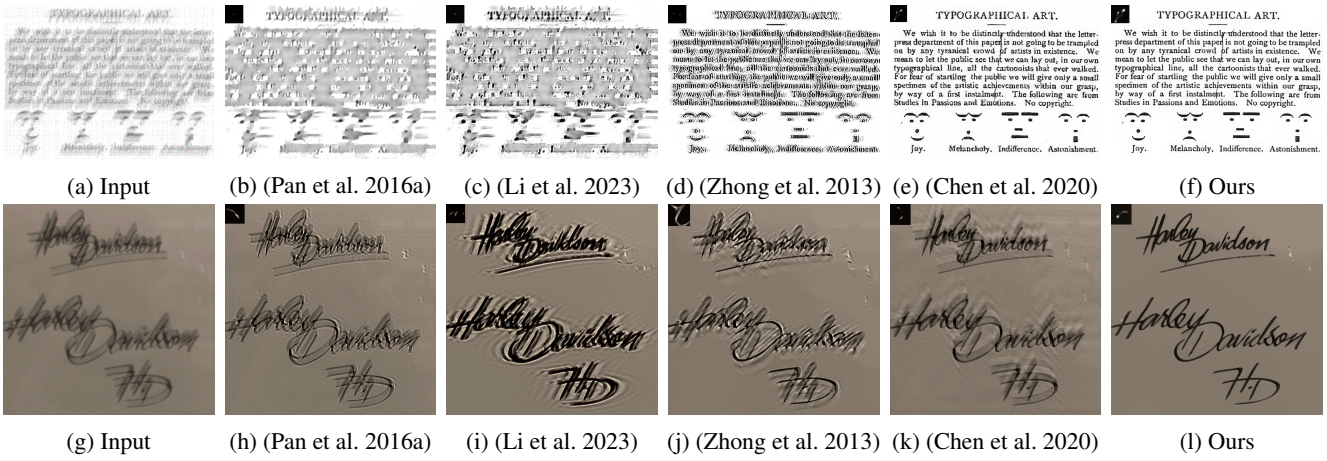

(a) Input (b) (Pan et al. 2016a) (c) (Li et al. 2023) (d) (Zhong et al. 2013) (e) (Chen et al. 2020) (f) Ours

(g) Input (h) (Pan et al. 2016a) (i) (Li et al. 2023) (j) (Zhong et al. 2013) (k) (Chen et al. 2020) (l) Ours

Figure 2: Visual Evaluation on Representative Text Blurry Images. The first example features an outlier proportion of 50%, whereas the second example involves a proportion of 10%.

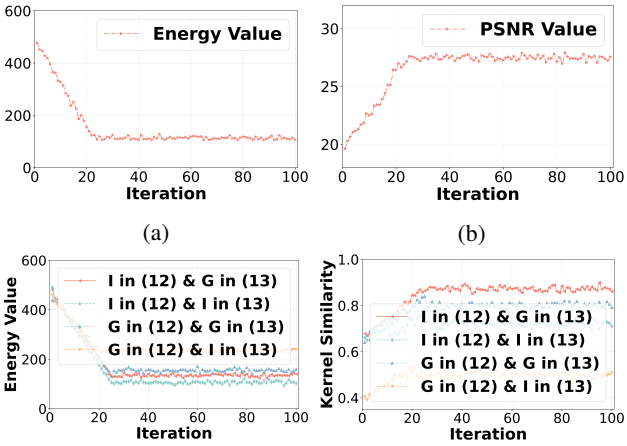

(a) (b) (c) (d)

Figure 3: Convergence analysis. (a) and (b) depict the convergence analysis of the proposed algorithm concerning the average energy of the objective function in (2) and the PSNR value, respectively. In (c) and (d), we assess various combinations of intensity and gradient formulations in (12) and (13), illustrating their impact on the average value of the energy function in (2) and the kernel similarity. Here, "I" and "G" represent "Intensity" and "Gradient", respectively.

ing image intensity for the data fidelity term in equation (12) and image gradient for the corresponding term in equation (13) outperforms the alternative configurations.

Furthermore, the proposed model employs three key parameters: γ_L, γ_K, and σ. To examine their impacts, we conducted experiments with varied settings while maintaining kernel similarity. γ_L was ranged from 10^{-5} to 0.01, γ_K from 0.02 to 5, and σ from 0 to 2. The results in Figure 4 demonstrate the robust performance of our algorithm across a broad parameter range in terms of γ_L, γ_K, and σ.

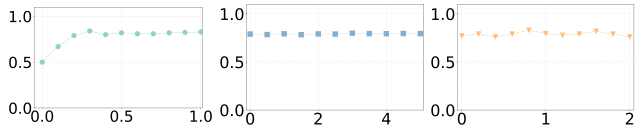

(a) $100 \cdot \gamma_L$ (b) γ_K (c) σ

Figure 4: Sensitivity analysis of γ_L (magnified by a factor of 100), γ_K, σ for proposed algorithm with respect to the kernel similarity metric.

Conclusion

In this paper, we have introduced a novel framework aimed at addressing the challenge of noisy text image deblurring. This innovative approach incorporates the concept of the maximum consensus framework, effectively distinguishing inliers from outliers by optimizing a pertinent quality metric, such as the inlier count. Additionally, we have seamlessly integrated the Alternating Direction Method of Multipliers (ADMM) and the Half-Quadratic Splitting (HQS) method to tackle the computationally demanding nature of the ℓ_0 norm. This pioneering strategy has yielded notable enhancements in the deblurring performance of text images afflicted by the presence of synthetic noise. Our proposed approach has been rigorously assessed through comprehensive experimental evaluations on noisy text blurry images. The empirical results consistently underscore the superior efficacy of our proposed method in the domain of noisy text image deblurring, surpassing the performance of existing methodologies. In future research, we intend to extend our algorithm's scope to encompass saturated images, natural scenes, and the challenges of non-uniform deblurring.

Acknowledgments

This research is supported by the BK21 Four Program (Pioneer Program in Next Generation Artificial Intelligence for Industrial Convergence, 5199991014250). We

express our appreciation to Augmented Knowledge Corp. (www.augmentedk.com) for their contributions to the development and experimentation resources. Additionally, we are grateful for the support of this work by the China Scholarship Council (CSC) (202008500123).

References

Boyd, S.; Parikh, N.; Chu, E.; Peleato, B.; Eckstein, J.; et al. 2011. Distributed optimization and statistical learning via the alternating direction method of multipliers. *Foundations and Trends® in Machine learning*, 3(1): 1–122.

Chakrabarti, A. 2016. A neural approach to blind motion deblurring. In *Computer Vision–ECCV 2016: 14th European Conference, Amsterdam, The Netherlands, October 11-14, 2016, Proceedings, Part III 14*, 221–235. Springer.

Chen, L.; Fang, F.; Zhang, J.; Liu, J.; and Zhang, G. 2020. Oid: Outlier identifying and discarding in blind image deblurring. In *Computer Vision–ECCV 2020: 16th European Conference, Glasgow, UK, August 23–28, 2020, Proceedings, Part XXV 16*, 598–613. Springer.

Cho, H.; Wang, J.; and Lee, S. 2012. Text image deblurring using text-specific properties. In *Computer Vision–ECCV 2012: 12th European Conference on Computer Vision, Florence, Italy, October 7-13, 2012, Proceedings, Part V 12*, 524–537. Springer.

Dong, J.; Pan, J.; Su, Z.; and Yang, M.-H. 2017. Blind image deblurring with outlier handling. In *Proceedings of the IEEE International Conference on Computer Vision*, 2478–2486.

Fang, X.; Zhou, Q.; Shen, J.; Jacquemin, C.; and Shao, L. 2018. Text image deblurring using kernel sparsity prior. *IEEE transactions on cybernetics*, 50(3): 997–1008.

Gong, D.; Yang, J.; Liu, L.; Zhang, Y.; Reid, I.; Shen, C.; Van Den Hengel, A.; and Shi, Q. 2017. From motion blur to motion flow: A deep learning solution for removing heterogeneous motion blur. In *Proceedings of the IEEE conference on computer vision and pattern recognition*, 2319–2328.

Huang, L.; Xia, Y.; and Ye, T. 2021. Effective blind image deblurring using matrix-variable optimization. *IEEE Transactions on Image Processing*, 30: 4653–4666.

Ji, S.-W.; Lee, J.; Kim, S.-W.; Hong, J.-P.; Baek, S.-J.; Jung, S.-W.; and Ko, S.-J. 2022. XYDeblur: divide and conquer for single image deblurring. In *Proceedings of the IEEE/CVF Conference on Computer Vision and Pattern Recognition*, 17421–17430.

Köhler, R.; Hirsch, M.; Mohler, B. J.; Schölkopf, B.; and Harmeling, S. 2012. Recording and Playback of Camera Shake: Benchmarking Blind Deconvolution with a Real-World Database. In *ECCV (7)*, 27–40.

Krishnan, D.; and Fergus, R. 2009. Fast image deconvolution using hyper-Laplacian priors. *Advances in neural information processing systems*, 22.

Krishnan, D.; Tay, T.; and Fergus, R. 2011. Blind deconvolution using a normalized sparsity measure. In *CVPR 2011*, 233–240. IEEE.

Kupyn, O.; Martyniuk, T.; Wu, J.; and Wang, Z. 2019. Deblurgan-v2: Deblurring (orders-of-magnitude) faster and better. In *Proceedings of the IEEE/CVF international conference on computer vision*, 8878–8887.

Levin, A.; Weiss, Y.; Durand, F.; and Freeman, W. T. 2009. Understanding and evaluating blind deconvolution algorithms. In *2009 IEEE conference on computer vision and pattern recognition*, 1964–1971. IEEE.

Levin, A.; Weiss, Y.; Durand, F.; and Freeman, W. T. 2011. Efficient marginal likelihood optimization in blind deconvolution. In *CVPR 2011*, 2657–2664. IEEE.

Li, Z.; Yang, M.; Cheng, L.; and Jia, X. 2023. Blind Text Image Deblurring Algorithm Based on Multi-Scale Fusion and Sparse Priors. *IEEE Access*, 11: 16042–16055.

Nah, S.; Hyun Kim, T.; and Mu Lee, K. 2017. Deep multi-scale convolutional neural network for dynamic scene deblurring. In *Proceedings of the IEEE conference on computer vision and pattern recognition*, 3883–3891.

Pan, J.; Hu, Z.; Su, Z.; and Yang, M.-H. 2016a. l_0-regularized intensity and gradient prior for deblurring text images and beyond. *IEEE transactions on pattern analysis and machine intelligence*, 39(2): 342–355.

Pan, J.; Lin, Z.; Su, Z.; and Yang, M.-H. 2016b. Robust kernel estimation with outliers handling for image deblurring. In *Proceedings of the IEEE Conference on Computer Vision and Pattern Recognition*, 2800–2808.

Qin, Z.; Wu, B.; and Li, M. 2018. Text Image Deblurring via Intensity Extremums Prior. In *International Conference on Multimedia Modeling*, 505–517. Springer.

Ravi, S. N.; Mehta, R.; and Singh, V. 2018. Robust blind deconvolution via mirror descent. *arXiv preprint arXiv:1803.08137*.

Tao, X.; Gao, H.; Shen, X.; Wang, J.; and Jia, J. 2018. Scale-recurrent network for deep image deblurring. In *Proceedings of the IEEE conference on computer vision and pattern recognition*, 8174–8182.

Vega, M.; Molina, R.; and Katsaggelos, A. K. 2014. Parameter estimation in Bayesian blind deconvolution with super Gaussian image priors. In *2014 22nd European Signal Processing Conference (EUSIPCO)*, 1632–1636. IEEE.

Xu, L.; and Jia, J. 2010. Two-phase kernel estimation for robust motion deblurring. In *Computer Vision–ECCV 2010: 11th European Conference on Computer Vision, Heraklion, Crete, Greece, September 5-11, 2010, Proceedings, Part I 11*, 157–170. Springer.

Xu, L.; Lu, C.; Xu, Y.; and Jia, J. 2011. Image smoothing via L 0 gradient minimization. In *Proceedings of the 2011 SIGGRAPH Asia conference*, 1–12.

Zhang, J.; Pan, J.; Ren, J.; Song, Y.; Bao, L.; Lau, R. W.; and Yang, M.-H. 2018. Dynamic scene deblurring using spatially variant recurrent neural networks. In *Proceedings of the IEEE conference on computer vision and pattern recognition*, 2521–2529.

Zhang, K.; Luo, W.; Zhong, Y.; Ma, L.; Stenger, B.; Liu, W.; and Li, H. 2020. Deblurring by realistic blurring. In *Proceedings of the IEEE/CVF Conference on Computer Vision and Pattern Recognition*, 2737–2746.

Zhong, L.; Cho, S.; Metaxas, D.; Paris, S.; and Wang, J. 2013. Handling noise in single image deblurring using directional filters. In *Proceedings of the IEEE conference on computer vision and pattern recognition*, 612–619.

Zhou, C.; Lin, S.; and Nayar, S. K. 2011. Coded Aperture Pairs for Depth from Defocus and Defocus Deblurring. *International journal of computer vision*, 93(1).